

Tuning band structures of photonic multilayers with positive and negative refractive index materials according to generalized Fibonacci and Thue–Morse sequences

Bruno P Silva[✉] and Carlos H Costa[✉]

Universidade Federal do Ceará, Campus Avançado de Russas, 62900-000, Russas—CE, Brazil

E-mail: carloshumberto@ufc.br

Received 23 August 2019, revised 13 November 2019

Accepted for publication 4 December 2019

Published 31 December 2019



Abstract

We investigate the photonic band structure, using the transfer-matrix method, in one-dimensional structures composed of a dispersive metamaterial A juxtaposed with a non-dispersive dielectric B according to the generalized Fibonacci and Thue–Morse sequences, which are ruled and characterized by two positive integer numbers, p and q . We present the band structures of different generations of these sequences for both TE and TM modes and discuss how they are affected by the p and q parameters and the ratio between the thicknesses of the building blocks. We obtain a new and very important analytical expression for the frequency in which the average refraction index vanishes, i.e. when the $\bar{n} = 0$ gap condition is satisfied, and we investigate, in detail, the behavior of this emergent scale insensitive gap, as a function of the thicknesses ratio, for all structures considered. For the metamaterial considered, we show that the reduced frequency for $\bar{n} = 0$ converges faster or slower to 0.41 depending on the sequence. By adjusting the p and q parameters, we can obtain a higher concentration of the pass bands inside (outside) the $n_A < 0$ region when there are more (less) blocks A than B in the unit cell. Our results also show the presence of omnidirectional and complete band gaps, which have various practical and technological applications.

Keywords: photonic quasicrystals, photonic band gaps, generalized Fibonacci sequence, generalized Thue–Morse sequence, metamaterials

(Some figures may appear in colour only in the online journal)

1. Introduction

Photonic crystals (PCs) are periodic structures that enable us to manipulate photon propagation [1] and, with the study of such materials, one can have full control of light in all electromagnetic spectra [2, 3]. This control is due to the spatial variation of the refractive index and, because of that, they display photonic bandgaps (PBGs), that are frequency regions where the wave-vector is complex and, as a consequence,

the electromagnetic wave is evanescent, so it is not allowed to propagate through the PC [4]. A great number of PCs can be found in nature (dielectrics and metals for example), but the left-handed materials, also called metamaterials, that was first theoretically proposed in 1964 by the Ukrainian physicist Victor Veselago [5], belong to a class of optical materials with very interesting optical properties and they are only artificially obtained (to a review see [6]). This kind of material has amazing features such as a left-handed triplet set of vectors \vec{k} , \vec{E} , \vec{H} , antiparallel wave and Poynting's vectors, the ability to

amplify evanescent waves, antiparallel phase and group velocities, simultaneously negative permittivity $\epsilon(\omega)$ and permeability $\mu(\omega)$ for a certain frequency range, therefore yielding a negative refractive index (NRI) $n = -\sqrt{|\epsilon(\omega)||\mu(\omega)|}$ [7], differently of the natural materials that present a positive refractive index (PRI). The NRI is exhibited by composites made of a periodic repetition of elementary ‘cells’ that consists of a split-ring resonator and a thin metallic wire, generating a negative effective permittivity and a negative effective permeability, respectively [8–10].

Regarding the applications of both PCs and metamaterials, they are widely used in an enormous variety of technological components such as lasers, guided waves, optical fibers, filters and computing, perfect lenses, Raman spectroscopy and solar cells [11–13]. Hence, their properties have been extensively studied by both theoretical and experimental research groups around the world, promising to lead us to the next age of technological devices based in optics [14].

Moreover, quasicrystals were discovered by Shechtman *et al* [15] in 1984 and they exhibit a pure point diffraction pattern like PCs but with a non-periodic arrangement and long-range order of its constituents. In one-dimensional (1D) systems, they can be constructed by two or more building blocks, represented by letters of the alphabet, following a substitution rule according some mathematical sequence: Fibonacci, Octonacci, Thue–Morse, double-period, for instance [16]. When light propagates in a given medium some internal degrees of freedom of the crystal are excited, giving rise to hybrid modes called polaritons. So, polaritons are quasiparticles consisting of a photon coupled with another elementary excitation such as a phonon for solids with elastic properties [17], a exciton for a electron–hole pair [18], a magnon for magnetic materials [19] and a plasmon for metallic composites [20] originating the phonon-polaritons, exciton-polaritons, magnon-polaritons and plasmon-polaritons, respectively. To a wide and deep review about polariton theory, the reader is encouraged to see [21] and the references therein. When a metamaterial is considered, the excited mixed modes are the plasmon-polaritons and they play a important role in the energy band structures, which are the most important sources of physical information about light propagation inside a given material. In this work, we intend to numerically obtain the band structures (frequency versus the wave-vector) of the considered superlattices in order to know how and when the light is allowed (bulk bands) or prohibited (band gaps) to propagate through the multilayered system.

In this work we will investigate the propagation of electromagnetic waves in 1D photonic quasicrystals (PQCs), where the spacial variation of the refractive index is given by a quasi-periodic mathematical sequence. The PQCs studied here are generated by the generalized Fibonacci [22] and Thue–Morse [23] sequences. These sequences are ruled by the following substitutional relations: $A \rightarrow B^q A^p$ and $B \rightarrow A$ (starting with B) for Fibonacci; and $A \rightarrow A^p B^q$ and $B \rightarrow A^q B^p$ (starting with A) for Thue–Morse. The letters A and B represent slabs of two different materials and the p and q parameters are positive and integer numbers. More mathematical details are given

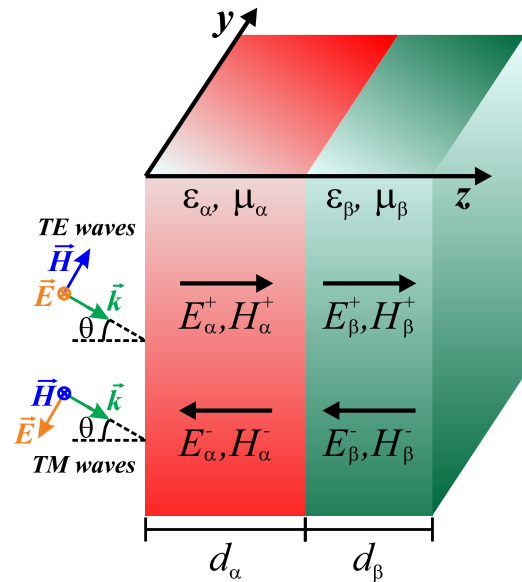


Figure 1. Schematic representation of the interface between two slabs, which correspond two different materials, with their respective physical (the electric permittivities and magnetic permeabilities) and geometrical (thicknesses of the layers) properties. Here, it is also presented the configurations of the TE and TM incident waves as well as the forward and backward electric and magnetic fields inside each layer.

later, and also can be found in [24, 25]. The constituents of the photonic superlattices are a frequency-dependent refractive index metamaterial (block A) and a non-dispersive and non-magnetic dielectric (block B). The theoretical model is based on Maxwell’s equations and the transfer-matrix method (TMM) [26] which significantly simplifies the algebra of this problem. In our results, we present the photonic band spectra for TE and TM obliquely incident waves and the frequencies for normally incident waves that allow light transmission as a function of the ratio of the thicknesses d_B/d_A for the first generations of the quasiperiodic sequences investigated here. This paper is organized as follows: in section 2, we present the theoretical approach used in this work, that are the 1D photonic structure together with Maxwell’s equations and the TMM in section 2.1, while the generalized Fibonacci and Thue–Morse quasicrystalline structures that were investigated, along with wide and deep comments about their most important properties are discussed in sections 2.2 and 2.3, respectively. The numerical results obtained as well as a discussion about the main observed results are presented in section 3, while our conclusions about the light propagation in the 1D photonic quasicrystals studied here are summarized in section 4.

2. The model

2.1. Maxwell’s equations and TMM

Here we employ the TMM that is a very simple and powerful technique to calculate the bulk band spectra of light propagation in 1D multilayered structures [26], besides, this method has a very good agreement with experimental results [27, 28]. In this work, the photonic crystal is composed by two

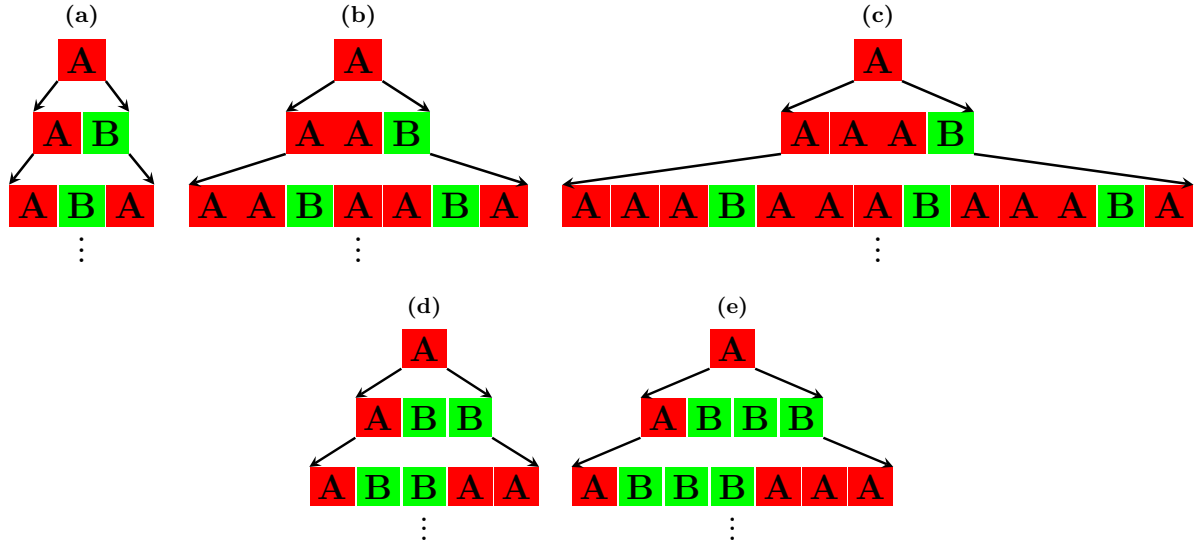


Figure 2. Generalized Fibonacci sequences: (a) Fibonacci GM or GFS(1,1); (b) Fibonacci SM or GFS(2,1); (c) Fibonacci BM or GFS(3,1); (d) Fibonacci CM or GFS(1,2); and (e) Fibonacci NM or GFS(1,3).

materials or media. The medium A is considered a metamaterial where the effective dispersive electrical permittivity and magnetic permeability are, respectively, given by

$$\epsilon_A(\omega) = 1 - \frac{\omega_p^2}{\omega^2}, \quad (1)$$

and

$$\mu_A(\omega) = 1 - F \frac{\omega^2}{\omega^2 - \omega_0^2}, \quad (2)$$

where $\omega_p/2\pi = 10$ GHz is the plasma frequency (which gives $\lambda_p = 2\pi c/\omega_p \approx 30$ mm, that is the plasma wavelength), $\omega_0/2\pi = 4$ GHz is the resonance frequency, and $F = 0.56$ is the fraction, whose value depends only on the geometry of the metamaterial [29, 30]. The medium B is a non-dispersive and non-magnetic dielectric, which is considered, on this work, composed by silicon dioxide (SiO_2), and the appropriated parameters for this material are $\epsilon_B = 12.3$, $\mu_B = 1$ [31]. For both materials, the refraction index is given by $n_\gamma = \sqrt{\epsilon_\gamma \mu_\gamma}$ (here and elsewhere, $\gamma = A$ or B). From equations (1) and (2), one can note that, for $\bar{\omega}_- < \bar{\omega} < \bar{\omega}_+$, both the electrical permittivity and the magnetic permeability of the metamaterial are negative, which gives us $n_A < 0$ [32], where $\bar{\omega} = \omega/\omega_p$ is the reduced frequency, $\bar{\omega}_-$ and $\bar{\omega}_+$ are, respectively, the lower and higher reduced frequencies where the NRI occurs. Taking into account the physical and geometrical parameters above cited, we have $\bar{\omega}_- = 0.4$ and $\bar{\omega}_+ = 0.6$. It is important to note that, for different materials and geometries, both $\bar{\omega}_-$ and $\bar{\omega}_+$ can assume different values [9].

We start the theoretical approach with a case which consists on finding a matrix that relates the amplitudes of the electric and magnetic fields of a light wave propagating inside a material A with the amplitudes of that wave in the juxtaposed material B . We solve Maxwell's equations together with the boundary conditions of both electric and magnetic fields at the interface in order to determine such matrix. Here, we consider

the case where both volumetric charge ρ and surface current \vec{J} densities are zero. The geometry of the problem, showed in figure 1, is such that the interface between the materials are in the $x - y$ plan (perpendicular to the z axis) and the wave-vector can propagate in the $x - z$ plan (perpendicular to the y axis). According to the geometry adopted in figure 1, the electric and magnetic fields are given by the superposition of forward and backward waves and they can be expressed in general by:

$$\vec{E}_\gamma(\vec{r}, t) = (0, E_{y\gamma}, 0), \quad (3)$$

with

$$E_{y\gamma} = (E_\gamma^+ e^{ik_\gamma z} + E_\gamma^- e^{-ik_\gamma z}) e^{ik_x x} e^{-i\omega t}, \quad (4)$$

for TE (or s -polarized) waves, and

$$\vec{H}_\gamma(\vec{r}, t) = (0, H_{y\gamma}, 0), \quad (5)$$

with

$$H_{y\gamma} = (H_\gamma^+ e^{ik_\gamma z} + H_\gamma^- e^{-ik_\gamma z}) e^{ik_x x} e^{-i\omega t}, \quad (6)$$

for TM (or p -polarized) waves. The magnetic field for TE polarization is obtained from equation (3) with $\vec{H} = -(i/\mu\omega)\vec{\nabla} \times \vec{E}$, while the electric field is obtained from equation (5) with $\vec{E} = (i/\epsilon\omega)\vec{\nabla} \times \vec{H}$. The superscript plus (minus) sign in equations (4) and (6) refer to the incident (reflected) fields. The wave-vector in medium γ is $\vec{k}_\gamma = (k_x, 0, k_{z\gamma})$, with $k_\gamma = n_\gamma \omega/c$. Thus, the x -component is $k_x = (n_\gamma \omega/c) \sin \theta_\gamma$, which is the Snell's law, while the z -component of the wave-vector is given by:

$$k_{z\gamma} = [k_\gamma^2 - k_x^2]^{1/2} = \left[\left(\frac{n_\gamma \omega}{c} \right)^2 - k_x^2 \right]^{1/2}. \quad (7)$$

Using Maxwell's equations together with the boundary conditions for both media and reorganizing the equation systems in a matrix form we obtain:

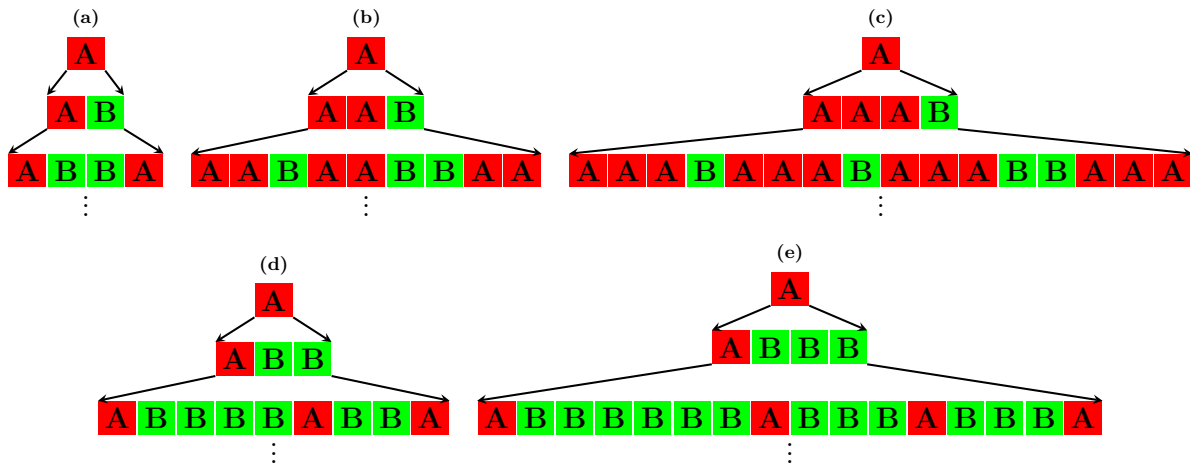


Figure 3. Generalized Thue–Morse sequences: (a) GTMS(1,1); (b) GTMS(2,1); (c) GTMS(3,1); (d) GTMS(1,2); and (e) GTMS(1,3).

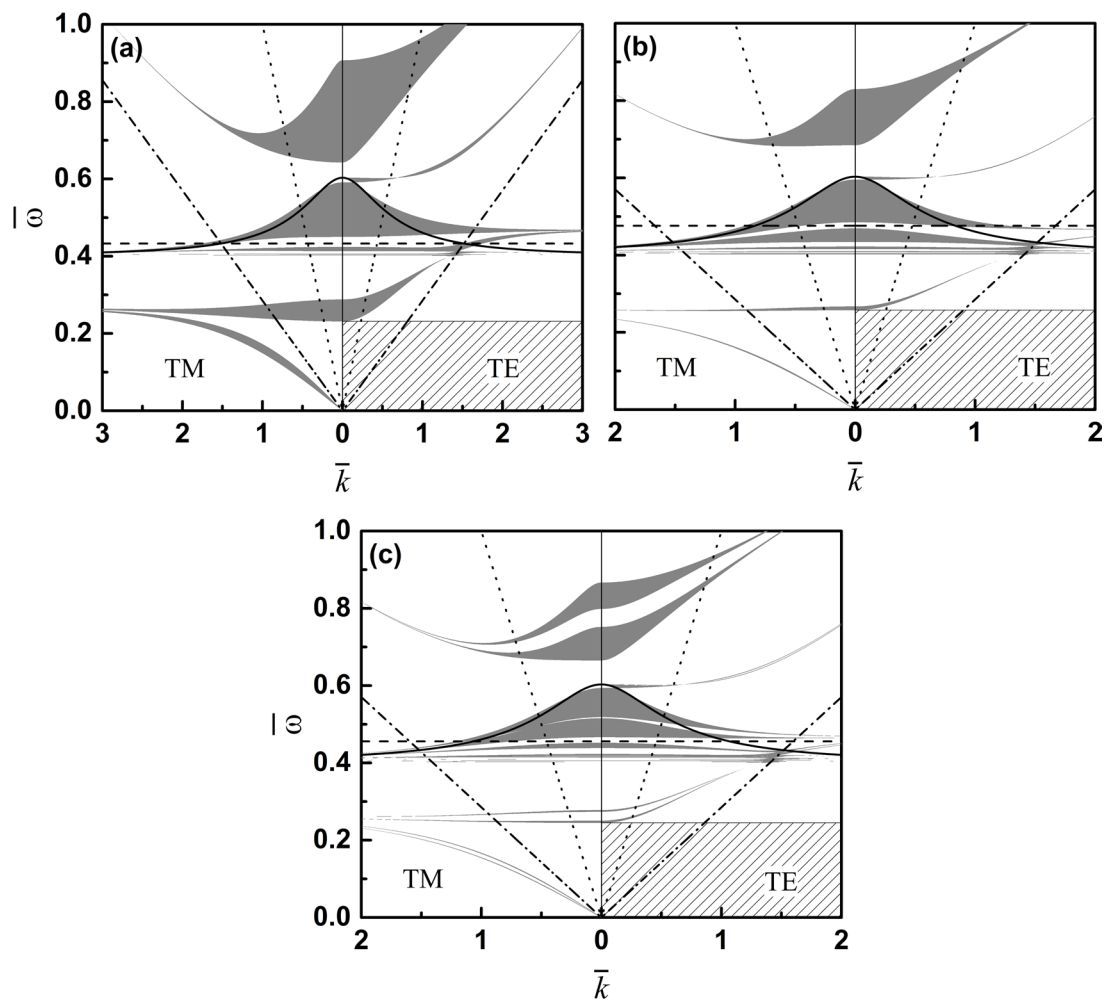


Figure 4. TE (right) and TM (left) photonic band spectra for a structure composed by a metamaterial A juxtaposed by a dielectric B for the (a) periodic case ($2GM = |A|B|$), (b) third ($3GM = |A|B|A|$) and (c) fourth ($4GM = |A|B|A|A|B|$) generations of the Fibonacci GM sequence. The light dispersion curves on vacuum ($\bar{\omega} = \bar{k}$) and on dielectric ($\bar{\omega} = \bar{k}/n_B$) are represented, respectively, by dotted and dash dotted lines. The solid line corresponds to the light dispersion relation for the metamaterial ($\bar{\omega} = \bar{k}/\sqrt{\epsilon_A\mu_A}$), while the horizontal dashed line, to the reduced frequency for which the $\bar{n} = 0$ gap condition, equation (14), is satisfied. Additionally, the hatched rectangle stands for the omnidirectional band gap frequency region.

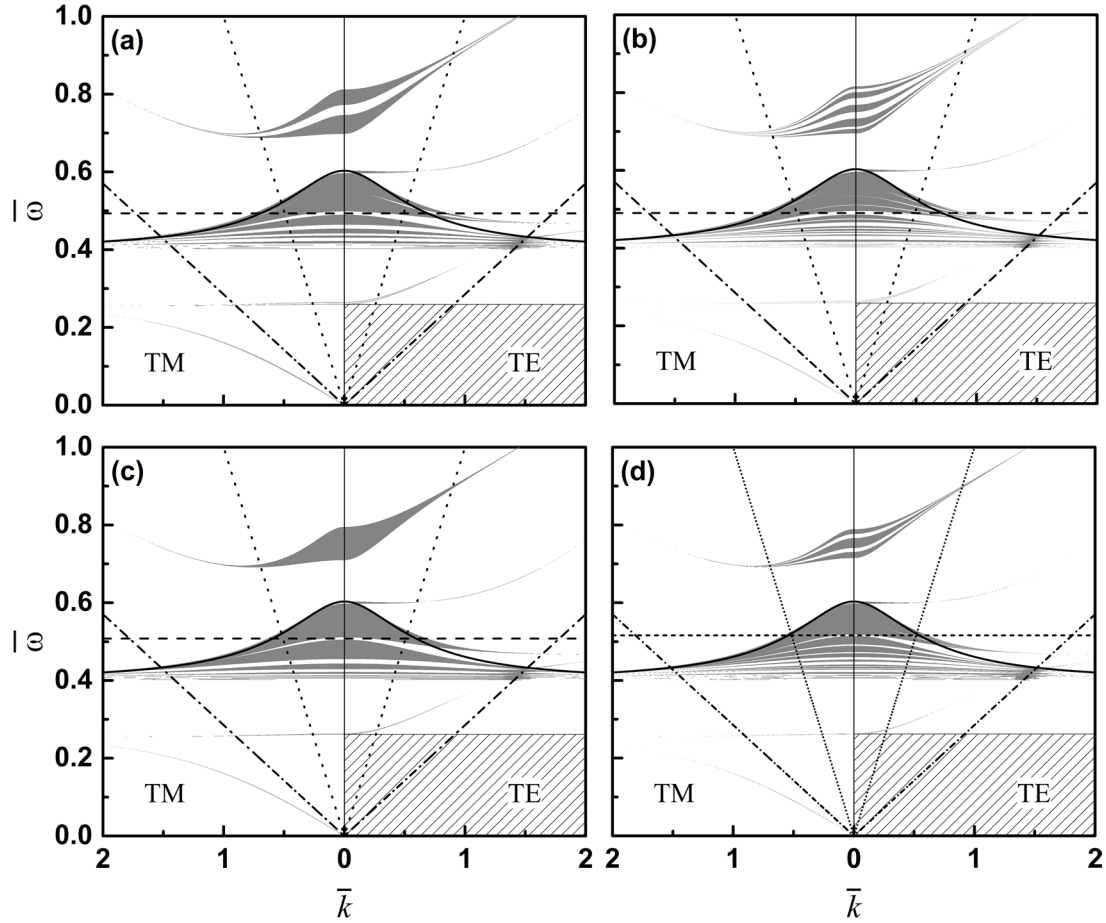


Figure 5. Same as figure 4, but for (a) third (3SM = $|A|A|B|A|A|B|A|$) and (b) fourth (4SM = $|A|A|B|A|A|B|A|A|A|B|A|A|B|A|A|B|A|A|B|$) generations of Fibonacci SM, and (c) second (2BM = $|A|A|A|B|$) and (d) third (3BM = $|A|A|A|B|A|A|A|B|A|A|A|B|A|$) generations of Fibonacci BM sequences.

$$\begin{pmatrix} E_{\beta}^{+} \\ E_{\beta}^{-} \end{pmatrix} = M_{\alpha\beta}^{\text{TE}} \begin{pmatrix} E_{\alpha}^{+} \\ E_{\alpha}^{-} \end{pmatrix}, \quad (8)$$

$$M_{\gamma} = \begin{bmatrix} \exp(ik_{z\gamma}d_{\gamma}) & 0 \\ 0 & \exp(-ik_{z\gamma}d_{\gamma}) \end{bmatrix}, \quad (12)$$

$$\begin{pmatrix} H_{\beta}^{+} \\ H_{\beta}^{-} \end{pmatrix} = M_{\alpha\beta}^{\text{TM}} \begin{pmatrix} H_{\alpha}^{+} \\ H_{\alpha}^{-} \end{pmatrix}, \quad (9)$$

where d_{γ} is the thickness of the respective material [30, 33].

where

For simplicity, if we consider a periodic photonic crystal with unit cell $|A|B|$, the transfer-matrix is $M = M_A M_{AB} M_B M_{BA}$ and it is a unimodular 2×2 matrix. The matrices M_{AB} and M_{BA} for TE and TM polarized waves are given by equations (10) and (11), respectively. Now, by using the Floquet–Bloch’s theorem, we obtain the dispersion relation for the electromagnetic waves in the form [34]:

$$M_{\alpha\beta}^{\text{TE}} = \frac{1}{2} \begin{bmatrix} 1 + \mu_{\beta\alpha}k_{z\alpha\beta} & 1 - \mu_{\beta\alpha}k_{z\alpha\beta} \\ 1 - \mu_{\beta\alpha}k_{z\alpha\beta} & 1 + \mu_{\beta\alpha}k_{z\alpha\beta} \end{bmatrix}, \quad (10)$$

$$2 \cos(QL) = \text{Tr}[M], \quad (13)$$

and

$$M_{\alpha\beta}^{\text{TM}} = \frac{1}{2} \begin{bmatrix} 1 + \epsilon_{\beta\alpha}k_{z\alpha\beta} & 1 - \epsilon_{\beta\alpha}k_{z\alpha\beta} \\ 1 - \epsilon_{\beta\alpha}k_{z\alpha\beta} & 1 + \epsilon_{\beta\alpha}k_{z\alpha\beta} \end{bmatrix}, \quad (11)$$

where $\text{Tr}[M]$ is the trace of the transfer-matrix M , Q is the Floquet–Bloch’s wave-vector, and L is the size of the unit cell (for the periodic case, $L = d_A + d_B$).

with $\alpha, \beta = A$ or B , $k_{z\alpha\beta} = k_{z\alpha}/k_{z\beta}$, $\epsilon_{\beta\alpha} = \epsilon_{\beta}/\epsilon_{\alpha}$ and $\mu_{\beta\alpha} = \mu_{\beta}/\mu_{\alpha}$. The matrices $M_{\alpha\beta}^{\text{TE}}$ and $M_{\alpha\beta}^{\text{TM}}$ are called the transmission matrices for TE and TM modes, respectively, because they relate the amplitudes of the fields when the wave crosses the interface from medium α to the medium β .

If we have a non-periodic arrangement of the slabs A and B , the light propagation will be strongly affected, resulting in new and very interesting photonic band structures. Besides, when we use a substitutional recurrence rule, it is known that the physical properties are changed and governed by the long-range correlations [21, 35]. In this work we investigate the light band structure in 1D PCs where the slabs A and B are spatially arranged in accordance with the generalized Fibonacci

On the other hand, the propagation of the light wave within of a layer γ , for both TE and TM waves, is characterized by the propagation matrix

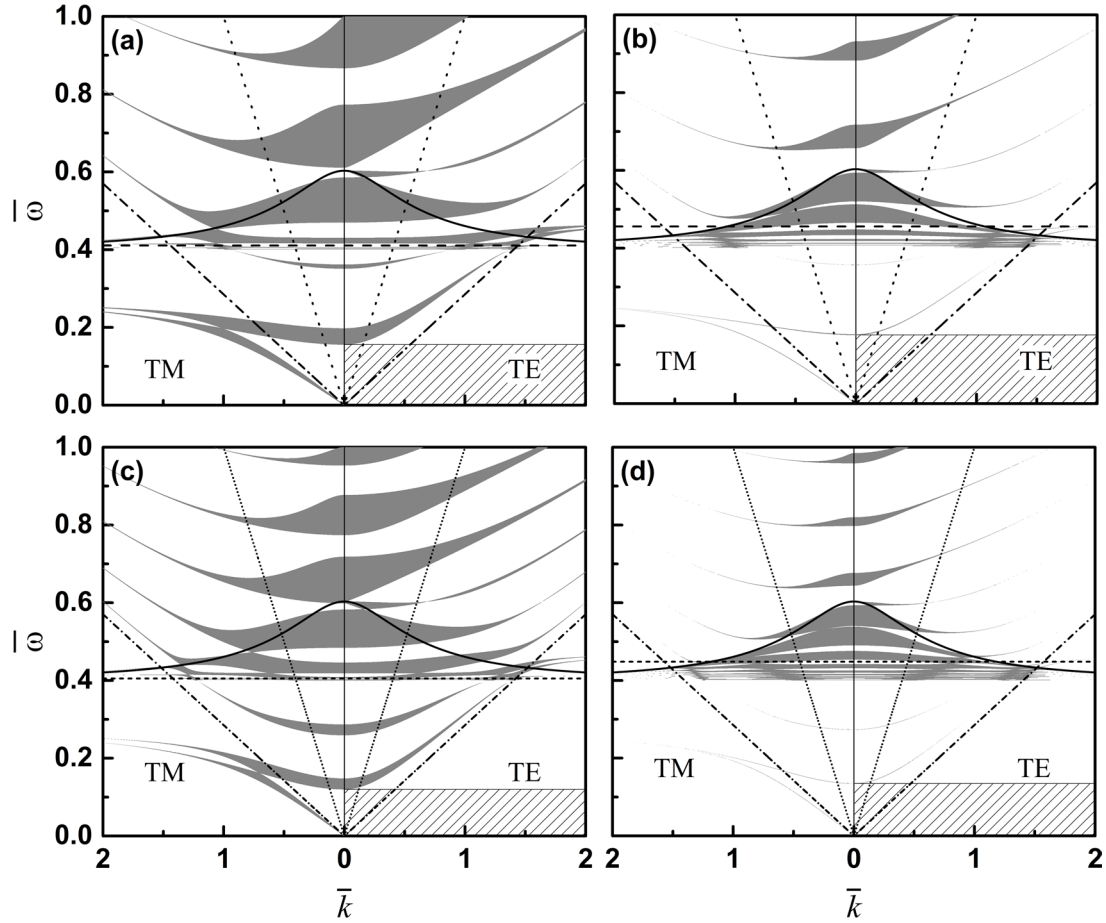


Figure 6. Same as figure 4, but for (a) second (2CM = |A|B|B|) and (b) third (3CM = |A|B|B|A|A|) generations of Fibonacci CM, and (c) second (2NM = |A|B|B|B|) and (d) third (3NM = |A|B|B|B|A|A|A|) generations of Fibonacci NM sequences.

and Thue–Morse sequences, because, by controlling only two integer parameters, p and q , one can obtain new and unconventional multilayers with a very rich and interesting photonic spectra. Also, by just adjusting the values of p and q , one can change the behavior of the whole structure. For example, considering N_A (N_B) as being the number of the slabs A (B) in a given unit cell, if $p > q$, we have $N_A > N_B$ and the photonic structures will be ruled by the physical properties of the metamaterial medium; otherwise, if $p < q$ implies $N_A < N_B$ and the photon propagation is dominated by the physical properties of the dielectric material as it will be observed from the numerical simulations.

Furthermore, we have the average refraction index that is given by:

$$\bar{n} = \frac{N_A n_A d_A + N_B n_B d_B}{N_A d_A + N_B d_B}. \quad (14)$$

Since we have a optical metamaterial that exhibits a NRI for given frequency range, there is always a wave frequency value

that turns the average refraction index equal to zero, forbidding light to cross the structure, in other words, there is always a gap that is called $\bar{n} = 0$ gap for this frequency value. This gap is of special interest because it can never be achieved by a PRI layered medium, where both refractive indexes are positive, and it does not change its position when both the widths d_A and d_B are rescaled by the same multiplicative factor, in contrast to the gaps in dielectric PCs [30]. By substituting equations (1) and (2) in (14), one obtain the following equation:

$$(1 - F - \Lambda^2) \bar{\omega}^4 + [(\Lambda^2 - 1) \omega_{0p}^2 - (1 - F)] \bar{\omega}^2 + \omega_{0p}^2 = 0, \quad (15)$$

where $\omega_{0p} = \omega_0/\omega_p$ and $\Lambda = -n_B(N_B/N_A)(d_B/d_A)$. One of the solutions of the above equation gives the frequencies that satisfy the condition $\bar{n} = 0$ as a function of the thicknesses ratio d_B/d_A . By inspection, for the metamaterial considered in this work, the only solution with physical meaning, i.e. the solution that provides positive frequencies, and satisfies the above mentioned condition is

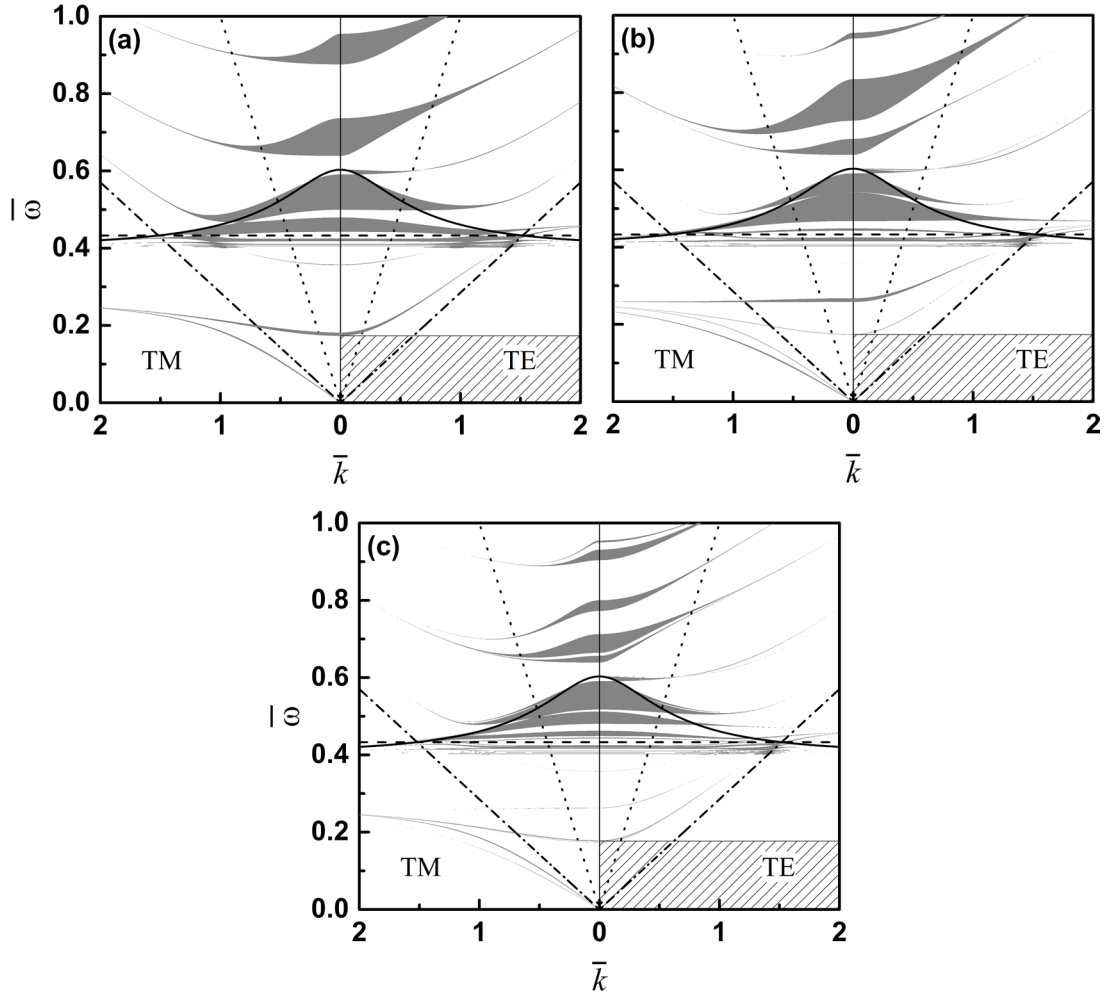


Figure 7. Same as figure 4, but for (a) second ($2\text{GTM}(1, 1) = |A|B|B|A|$), (b) third ($3\text{GTM}(1, 1) = |A|B|B|A|B|A|A|B|$) and (c) fourth ($4\text{GTM}(1, 1) = |A|B|B|A|B|A|A|B|B|A|A|B|A|B|B|A|$) generations of GTM(1,1) sequence.

$$\bar{\omega} = \left\{ \frac{\left[(\Lambda^2 - 1) \omega_{0p}^2 - (1 - F) \right] + \sqrt{\left[(\Lambda^2 - 1) \omega_{0p}^2 - (1 - F) \right]^2 + 4 (\Lambda^2 + F - 1) \omega_{0p}^2}}{2 (\Lambda^2 + F - 1)} \right\}^{1/2}. \quad (16)$$

It is important to note that the $\bar{n} = 0$ gap is a single frequency gap, however, Kocaman and co-workers reported, for the first time, that the $\bar{n} = 0$ gap can emerge in artificial superlattices with remarkable agreement with numerical simulations and such structures can be used for complete wavefront control for arbitrary phase delay lines [36, 37].

On the next two subsections we present and discuss in more details the generalized Fibonacci and Thue–Morse sequences.

2.2. Generalized Fibonacci sequences

The first class of quasiperiodic systems studied here are the multilayers built according to the generalized Fibonacci sequences (GFSs), whose their five most famous generalizations are known as the metallic numbers or mean family: golden mean (GM), which is the usual Fibonacci sequence,

silver mean (SM), bronze mean (BM), copper mean (CM) and nickel mean (NM). This family of sequences and their mathematical and physical properties are defined by the generalized Fibonacci substitution matrix S_{GF} [25]:

$$S_{\text{GF}} = \begin{pmatrix} p & q \\ 1 & 0 \end{pmatrix}, \quad (17)$$

where p and q are positive integers here and elsewhere. The characteristic value of the GFSs, $\sigma_{\text{GF}}(p, q)$, represents the ratio between the number of building blocks in the j th generation and the number of building blocks in the $(j - 1)$ th generation in the limit $j \rightarrow \infty$. This value is defined by the positive solution of the quadratic equation (characteristic equation of the matrix S_{GF}) [22]:

$$\sigma_{\text{GF}}^2 - p\sigma_{\text{GF}} - q = 0, \quad (18)$$

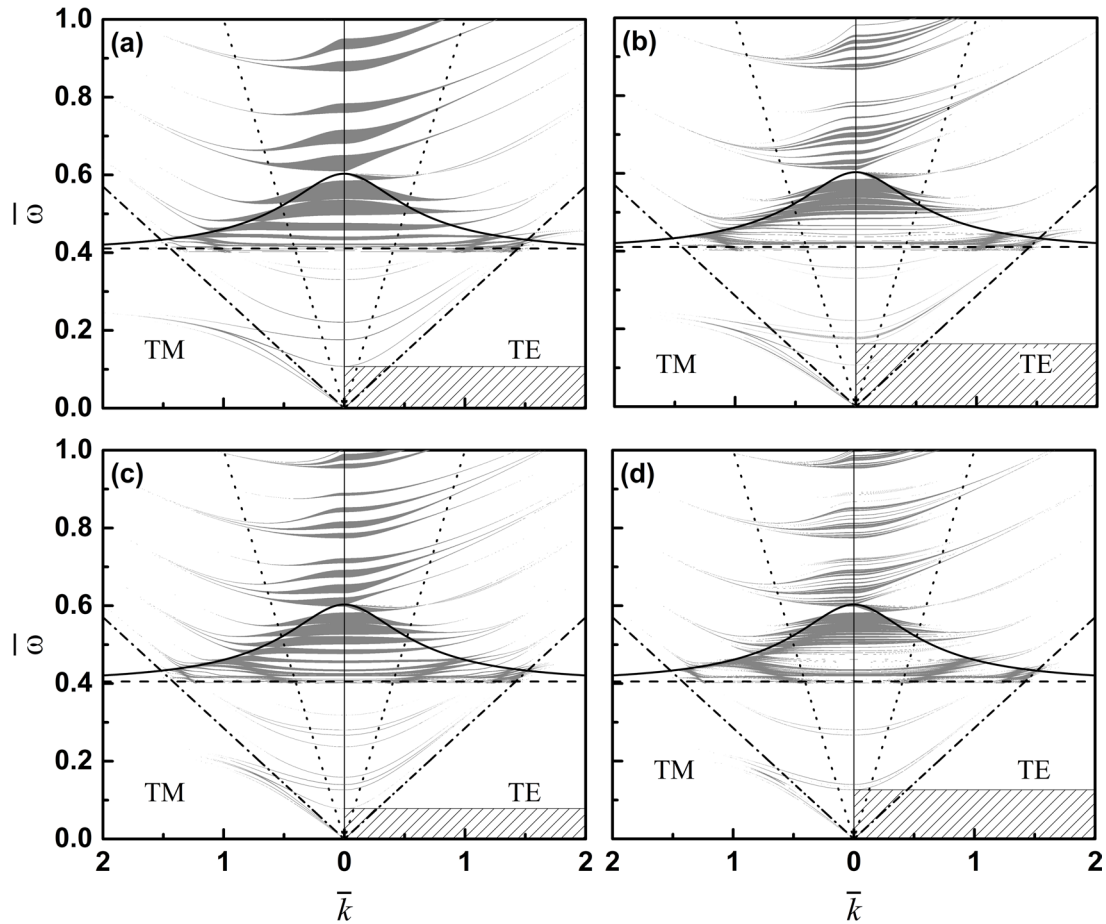


Figure 9. Same as figure 4, but for (a) second ($2\text{GTM}(1, 2) = |A|B|B|B|B|A|B|B|A|$) and (b) third ($3\text{GTM}(1, 2) = |A|B|B|B|B|B|A|B|B|B|B|A|B|B|B|B|A|B|B|A|A|B|B|B|B|B|A|B|B|B| \dots \dots |A|A|B|B|B|$) generations of $\text{GTM}(1,2)$, (c) second ($2\text{GTM}(1, 3) = |A|B|B|B|B|B|B|B|A|B|B|B|B|A|B|B|B|A|$) and (d) third generations of $\text{GTM}(1,3)$ sequences (We do not specify the unit cell of the $3\text{GTM}(1,3)$ because it contains 64 slabs. The reader can obtain the structure from equations (25) and (26)).

Table 1. Frequency values in which the condition of the $\bar{n} = 0$ gap is satisfied.

Sequence	$\bar{\omega}$	ω (GHz)	Sequence	$\bar{\omega}$	ω (GHz)
2GM	0.43	27.02	3CM	0.46	28.90
3GM	0.48	30.16	2NM	0.41	25.76
4GM	0.46	28.90	3NM	0.45	28.27
3SM	0.49	30.79	TM(1,1)	0.43	27.02
4SM	0.49	30.79	TM(2,1)	0.48	30.16
2BM	0.51	32.04	TM(3,1)	0.51	32.04
3BM	0.52	32.67	TM(1,2)	0.11	6.91
2CM	0.41	25.76	TM(1,3)	0.08	5.03

Table 2. Frequency values in which there is an omnidirectional band gap in TE modes from 0 until ω .

Sequence	$\bar{\omega}$	ω (GHz)	Sequence	$\bar{\omega}$	ω (GHz)
2GM	0.23	14.45	2TM(1,1)	0.17	10.68
3GM	0.26	16.34	3TM(1,1)	0.17	10.68
4GM	0.25	15.71	4TM(1,1)	0.18	11.31
3SM	0.26	16.34	2TM(2,1)	0.18	11.31
4SM	0.26	16.34	3TM(2,1)	0.26	16.34
2BM	0.26	16.34	2TM(3,1) ^a	0.4	25.13
3BM	0.26	16.34	3TM(3,1) ^a	0.4	25.13
2CM	0.16	10.05	2TM(1,2)	0.11	6.91
3CM	0.18	11.31	3TM(1,2)	0.16	10.05
2NM	0.12	7.54	2TM(1,3)	0.08	5.03
3NM	0.13	8.17	3TM(1,3)	0.13	8.17

^a Indicates the occurrence of the complete band gap.

S regardless the chosen inflation (or recurrence) rule. One interesting curiosity is that the SM sequence presented here is equivalent (has the same substitution matrix, and therefore the same properties) to the Octonacci sequence and if one choose a non-common substitution rule like the one presented in [16], one can easily see that the obtained structure is exactly equal to the structure formed by the SM sequence.

2.3. Generalized Thue–Morse sequences

The second class of quasiperiodic systems studied in this work are the superlattices formed according the generalized Thue–Morse sequences (GTMSs). Likewise the GFSs,

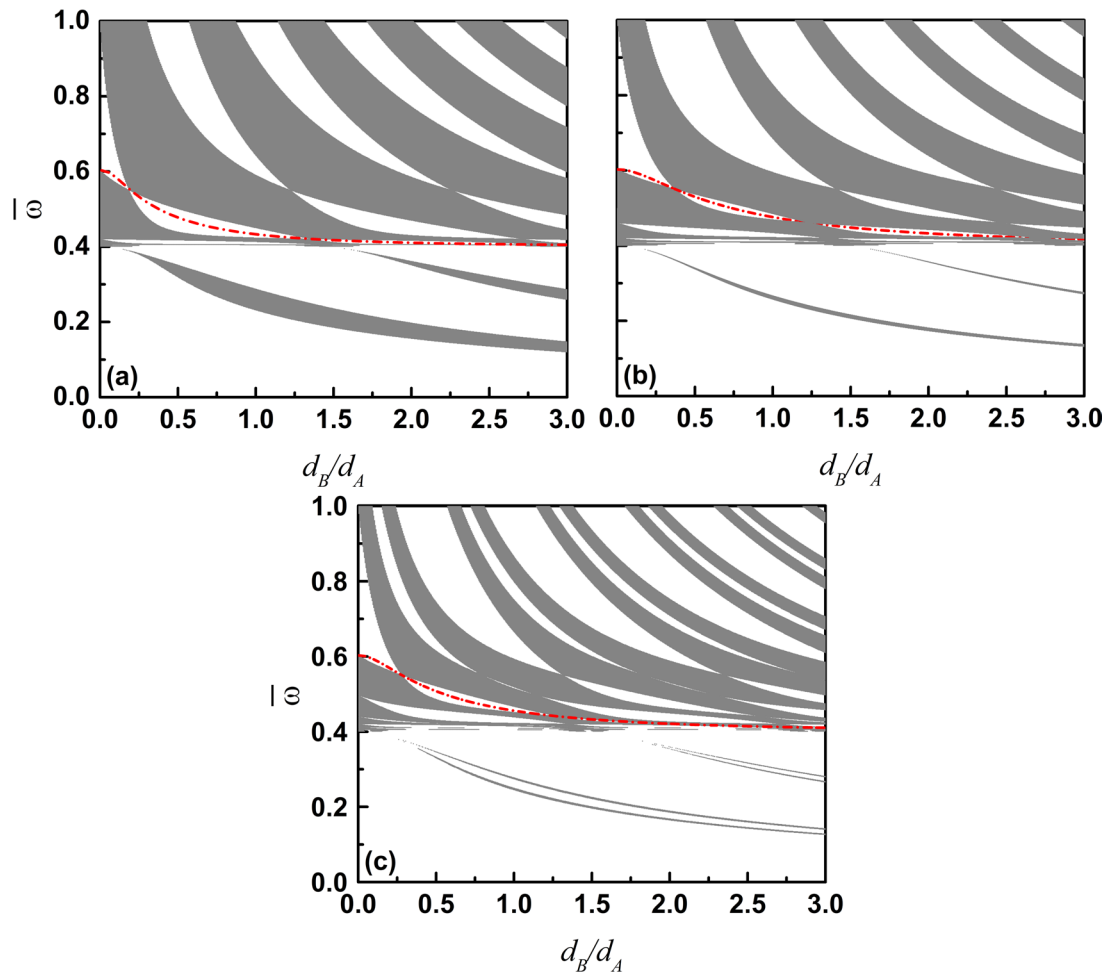


Figure 10. Reduced frequency versus relative width of the medium d_B/d_A for (a) periodic case, (b) third and (c) fourth Fibonacci GM sequence. The red dotted-dashed line represents the frequencies where $\bar{n} = 0$ gaps as a function of the ratio d_B/d_A , which is the plot of equation (16).

the mathematical and physical properties of the GTMSs are defined by the substitution matrix S_{GTMS} :

$$S_{\text{GTMS}} = \begin{pmatrix} p & q \\ p & q \end{pmatrix}. \quad (23)$$

The ratio between the number of building blocks in the j th generation and the number of building blocks in the $(j - 1)$ th generation of the GTMSs is defined by:

$$\sigma_{\text{GTMS}}(p, q) = \frac{\text{TM}_j(p, q)}{\text{TM}_{j-1}(p, q)} = p + q \quad (24)$$

which is also the solution of the characteristic equation, where $\text{TM}_j(p, q) = (p + q)^j$ is the total number of building block on the j th generation (see more details in [24]). Unlike the GFSs, where a irrational ratio can be obtained, this ratio is always constant and integer. Furthermore, the ratio between the number of blocks A (N_A) and the number of blocks B (N_B) is constant too, depending only on the numbers p and q on the generation of the given sequence, that is, $N_A/N_B = p/q$ for any of the GTMSs. That leads to an invariant frequency in with occurs the $\bar{n} = 0$ gap for each of the sequences, that is verified in our numerical calculations showed in section 3.

One can construct the quasiperiodic lattice according the GTMSs by using S_{GTMS} which gives the following inflation rule:

$$\begin{pmatrix} A \\ B \end{pmatrix} \rightarrow \begin{pmatrix} p & q \\ p & q \end{pmatrix} \begin{pmatrix} A \\ B \end{pmatrix} = \begin{pmatrix} A^p B^q \\ B^q A^p \end{pmatrix} \quad (25)$$

or

$$A \rightarrow A^p B^q \quad \text{and} \quad B \rightarrow B^q A^p \quad (26)$$

where A^p (B^q) has the same meaning as for the GFSs. The usual Thue–Morse sequence (UTMS) is recovered when $p = q = 1$, then, the inflation rule becomes: $A \rightarrow AB$ and $B \rightarrow BA$ [39]. Another way to construct superlattices according the UTMS is from a recurrence rule in such a way that the j th generation is given by:

$$S_j = S_{j-1} \bar{S}_{j-1} \quad (j \geq 1), \quad (27)$$

where $S_0 = A$, \bar{S}_{j-1} is obtained from S_{j-1} by replacing A for B and vice-versa. In figure 3 it is shown the growth of the generalized Thue–Morse sequences from $j = 0$ to $j = 2$.

The structures constructed following the UTMS have a purely singular continuous spectra for both energy and

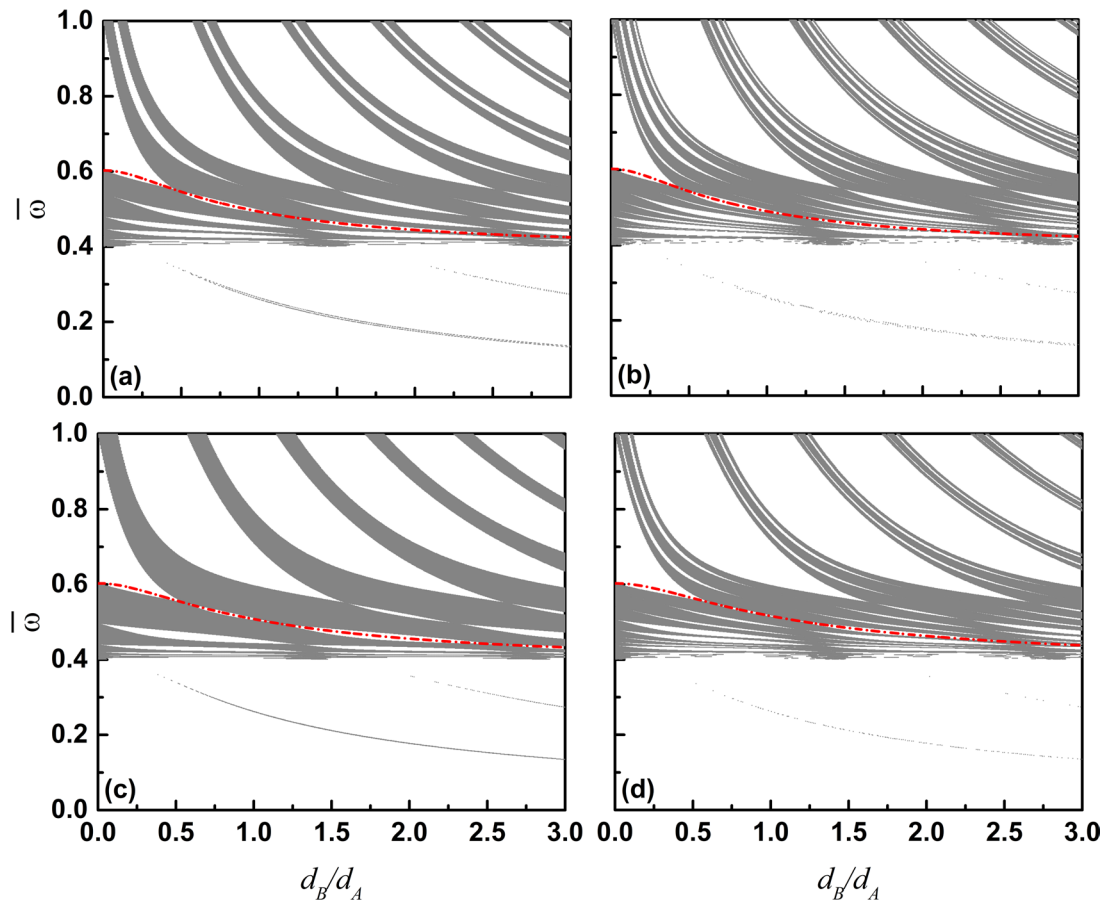


Figure 11. Reduced frequency versus relative width of the medium d_B/d_A for (a) third and (b) fourth generations of Fibonacci SM, and (c) second and (d) third generations of Fibonacci BM sequences.

Fourier spectrum, therefore, they have a degree of disorder between quasiperiodic and random lattices, the first one characterized, likewise periodic structures, by δ -function peaks in the Fourier spectra, and the later by a absolutely continuous Fourier spectra. Again, to a review of the subject see [38]. The UTMS is self-similar, thus, the translational symmetry has been replaced by a invariance with respect to multiplicative changes of scale, or scaling invariance, with the scaling factor being equal to 2. That type of symmetry is nothing but periodicity on a logarithmic scale [24].

3. Numerical results

In this section, we present the numerical results regarding the light wave propagation in 1D PQC's whose spatial arrangement of the building blocks A and B are in accordance to the GFS and GTMS. The thicknesses of the materials are $d_A = d_B = \lambda_p/4 \approx 7.5$ mm.

In figure 4(a) we present the plot of the reduced frequency, $\bar{\omega} = \omega/\omega_p$, versus the reduced wave-vector, $\bar{k} = k_x/k_p$, showing the allowed bulk bands (gray shaded areas) and the band gaps (white areas) for the periodic case, which also correspond to the second generation of the Fibonacci GM sequence, whose unit cell is $2GM = |A|B|$. We have the bulk bands for the TM modes (or p -polarized waves) on left, while the TE modes (or s -polarized waves) are displayed on

right. For TE polarization, one can see that for $\bar{\omega} < 0.23$ (or $\omega < 14.45$ GHz), this configuration display a omnidirectional band gap, which is a frequency region where the wave is not allowed to propagate through the PC independently of the incident angle. As for the TM polarization, we have propagating waves, so that structure can be used to construct ‘on or off’ devices by just changing the polarization of the light wave [11, 40–44]. Those bands occur due to the overlap of surface waves at the interface of the metamaterial-dielectric [30, 45]. Additionally, for both TE and TM modes we see backward waves in the frequency region $0.4 < \bar{\omega} < 0.6$ that are characterized by a negative slope of the allowed photonic band. Those waves can also be seen in TM modes for $\bar{\omega} > 0.6$ but around $\bar{k} = 1$ they turn into forward waves, that are identified by the positive slope of the branches.

For the $n_A < 0$ region, there are two types of gaps: one is the $\bar{n} = 0$ gap, which happens in the reduced frequency of $\bar{\omega} \approx 0.43$ (or $\omega \approx 27.02$ GHz), and it is represented in figure 4(a) by the horizontal dashed line; the other gaps are the well-known Bragg’s gaps, which occur due to the destructive interference provoked by the scattering of the propagating waves inside the structure. For $\bar{\omega} > 0.6$, one can see one branch for each polarizations. For TE modes it has a positive slope which means that the energy flux is in the same direction as the propagation of light, in contrast with the branch for the TM modes that present a negative slope, meaning a energy

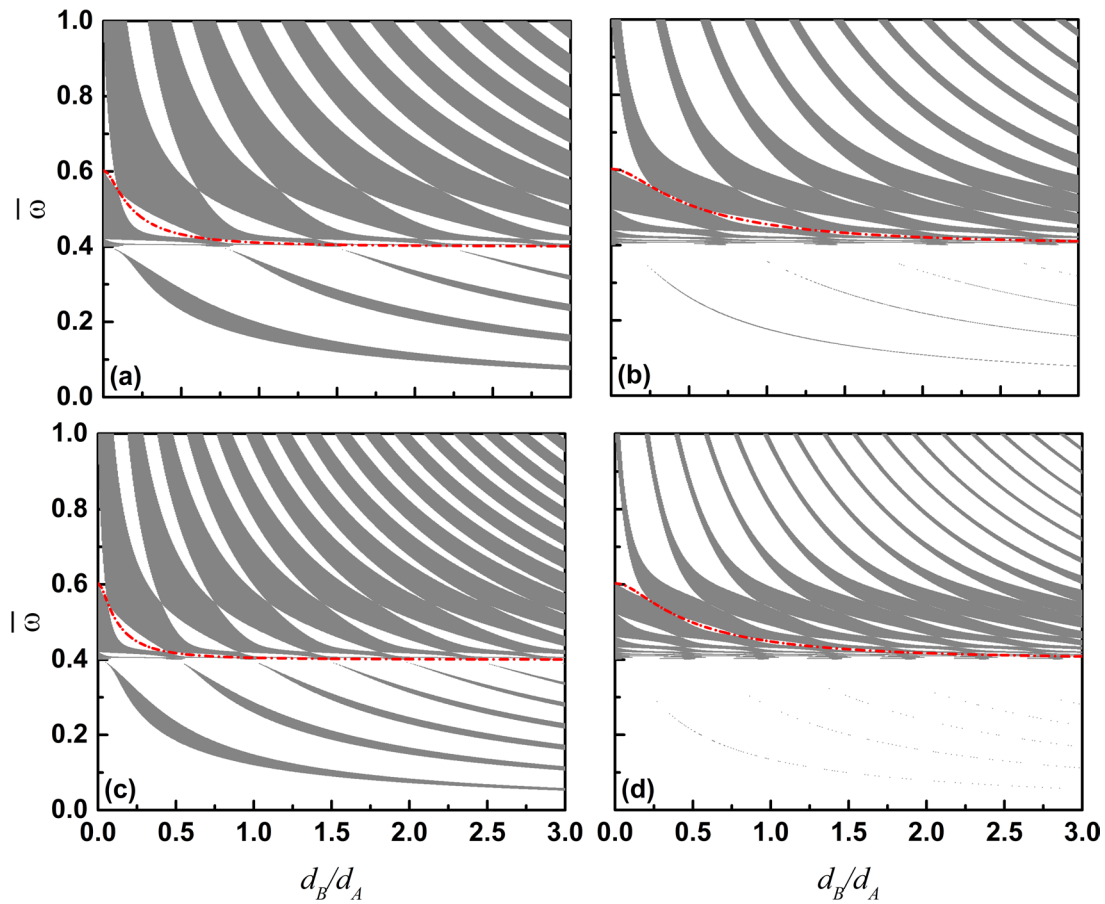


Figure 12. Reduced frequency versus relative width of the medium d_B/d_A for (a) second and (b) third generations of Fibonacci CM, and (c) second and (d) third generations of Fibonacci NM sequences.

flux in an opposite direction to the propagation of light, which is characteristic of a structure composed by metamaterials.

In figures 4(b) and (c) we show the photonic band structures same as in figure 4(a), but now for the third and fourth generations of the Fibonacci GM sequence, whose unit cells are $3GM = |A|B|A|$ and $4GM = |A|B|A|A|B|$, respectively. The frequency regions of occurrence of the omnidirectional band gap are $\bar{\omega} < 0.26$ for third and $\bar{\omega} < 0.25$ (or $\omega < 16.34$ GHz and $\omega < 15.71$ GHz, respectively) for fourth generations. In the $n_A < 0$ region the frequency in which the $\bar{n} = 0$ gap appears are $\bar{\omega} \approx 0.48$ for third and $\bar{\omega} \approx 0.46$ for fourth generations (or $\omega \approx 30.16$ GHz and 28.90 GHz, respectively). As expected, all the bands get narrow and narrow and the spectra become more fragmented due to the more complex arrange of unit cell of the structure as a consequence of the long-range correlations induced by the substitutional relations [22].

In figure 5 we see the same as in figure 4, but now for the third (figure 5(a)) and fourth (figure 5(b)) generations of Fibonacci SM sequence, and the unit cells are $3SM = |A|A|B|A|A|B|A|$ and $4SM = |A|A|B|A|A|B|A|A|B|A|A|B|A|A|B|A|A|B|$, respectively. The second generation of the SM sequence is not shown here because it is physically identical to the third generation of the GM sequence (the unit cells are $2SM = |A|A|B|$ and $3GM = |A|B|A|$) which has already been presented in figure 4(b). The photonic band structure for the second and third generations of the Fibonacci BM sequence are

presented in figures 5(c) and (d), and whose unit cells are $2BM = |A|A|A|B|$, and $3BM = |A|A|A|B|A|A|A|B|A|A|A|B|A|$, respectively. In all these figures one can clearly observe a more fragmented spectra, specially in the $n_A < 0$ region.

Also from figure 5, the frequency region of the omnidirectional band gap is $\bar{\omega} < 0.26$ (or $\omega < 16.34$ GHz) for all sequences, i.e. 3SM, 4SM, 2BM and 3BM. Additionally, the frequencies for which the $\bar{n} = 0$ gap emerges are $\bar{\omega} \approx 0.49$ for both third and fourth generations of SM sequence, while $\bar{\omega} \approx 0.51$ for second and $\bar{\omega} \approx 0.52$ for third generations of BM sequence (or $\omega \approx 30.79$, 32.04 and 32.67 GHz, respectively). Besides, as expected, we have more narrower and fragmented bulk bands in SM and CM structures than in GM ones, and these new bands emerge mostly in a frequency region where $n_A < 0$ because in GM, SM and BM sequences we have more building blocks A than B, i.e. $N_A > N_B$ for these sequences, so that the physical properties of the metamaterial dominates and the whole structure behave as such.

In figure 6 we plot the photonic band structures for second and third generations of the Fibonacci CM (figures 6(a) and (b), respectively) and of the Fibonacci NM (figures 6(c) and (d), respectively) sequences. The unit cells of these PQC are $2CM = |A|B|B|$, $3CM = |A|B|B|A|A|$, $2NM = |A|B|B|B|$ and $3NM = |A|B|B|B|A|A|A|$. Here, we see a quite different and a very interesting pattern of the bulk bands that were presented until now. For frequencies below the resonant one, namely

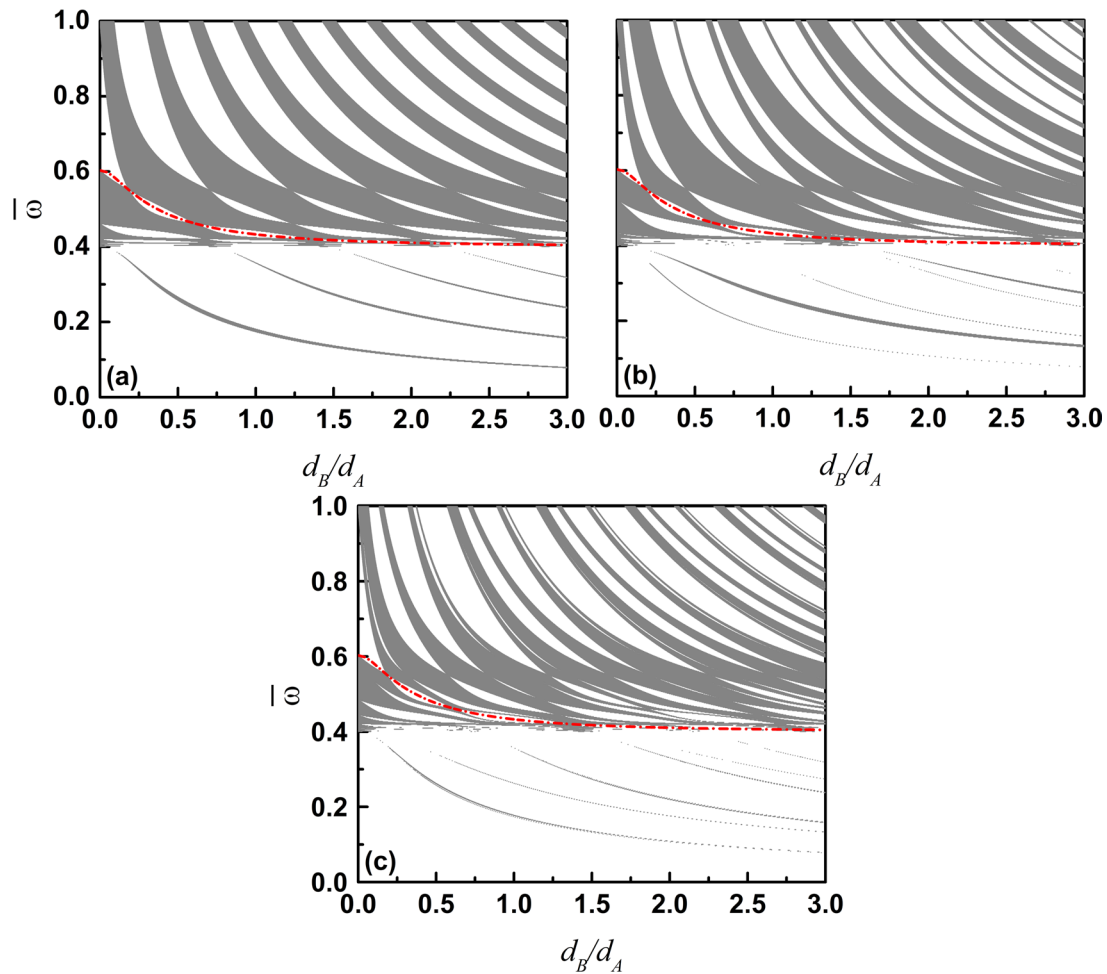


Figure 13. Same as figure 10, but for (a) second, (b) third and (c) fourth generations of Thue–Morse (1,1) sequence.

$\bar{\omega} < 0.4$, the band structures present a similar behavior as in figure 4 with some allowed bands for both TE and TM waves. However, for $\bar{\omega} > 0.4$, one can see that the waves start as backward waves and, for a given value of the reduced wavelength, they turn into forward waves for TM and some TE modes, even in the $n_A < 0$ region. This occurs because of the strong influence of the physical properties of the dielectric slab in the whole photonic structure for the CM and NM sequences, whose unit cells have, in general, a number of building blocks B bigger or, at least, equal to the A ones.

From figure 6, we can also observe that the $\bar{n} = 0$ gap condition is satisfied for $\bar{\omega} \approx 0.41$ ($\omega \approx 25.76$ GHz) for second, and $\bar{\omega} \approx 0.46$ ($\omega \approx 28.90$ GHz) for third generations of CM sequence while the omnidirectional gap in TE modes is in the frequency region $\bar{\omega} < 0.16$ ($\omega < 10.05$ GHz) for second and $\bar{\omega} < 0.18$ ($\omega < 11.31$ GHz) for third generations of that same sequence. As for the NM sequence, we have the $\bar{n} = 0$ gap located in $\bar{\omega} \approx 0.41$ ($\omega \approx 25.76$ GHz) and $\bar{\omega} \approx 0.45$ ($\omega \approx 28.27$ GHz) while the omnidirectional gap is in $\bar{\omega} < 0.12$ ($\omega < 7.54$ GHz) and $\bar{\omega} < 0.13$ ($\omega < 8.17$ GHz) for second and third generations, respectively. Besides, it is important to mention that, as expected, in this figure we have more and narrower allowed bands than in figures 4 and 5 for the same generation number because of the increase in the number of blocks in the unit cells (see figures 4(b), 5(a), 5(c),

6(b) and 6(d)). However, a remarkable result is that the new bands now emerge outside of the $n_A(\omega) < 0$ region due to the increase of dielectric slabs in the unit cells.

Now, we present some results regarding the light propagation in PQC's built in accordance with the generalized Thue–Morse sequences. Some lower generations of the GTMS's correspond to some structures formed by the GFS's already presented. Namely, the first generation of the GTM(1,1), GTM(2,1), GTM(3,1), GTM(1,2) and GTM(1,3) correspond to the second generation of the GM, SM, BM, CM and NM sequences, respectively, and, because of that, they are not presented here.

In figure 7(a) we show the photonic band structure for a multilayer constructed according the second generation of the UTMS, named 2GTM(1,1), whose unit cell is $|A|B|B|A|$. From it, one can see a omnidirectional band gap for the TE modes for frequency range $\bar{\omega} < 0.17$ (or $\omega < 10.68$ GHz), in contrast with the TM modes where exists a branch of propagating waves and therefore, for that frequency range, this structure can also be applied on optical logical devices. For $\bar{\omega} \approx 0.18$ (or $\omega \approx 11.31$ GHz), a branch emerges for both TE and TM modes, and the TM branch get together with the lower one and they go asymptotically to the value $\bar{\omega} \approx 0.25$ (or $\omega \approx 15.71$ GHz), while the branch for TE waves goes asymptotically with the dielectric light line. In the $n_A < 0$ region, for a certain

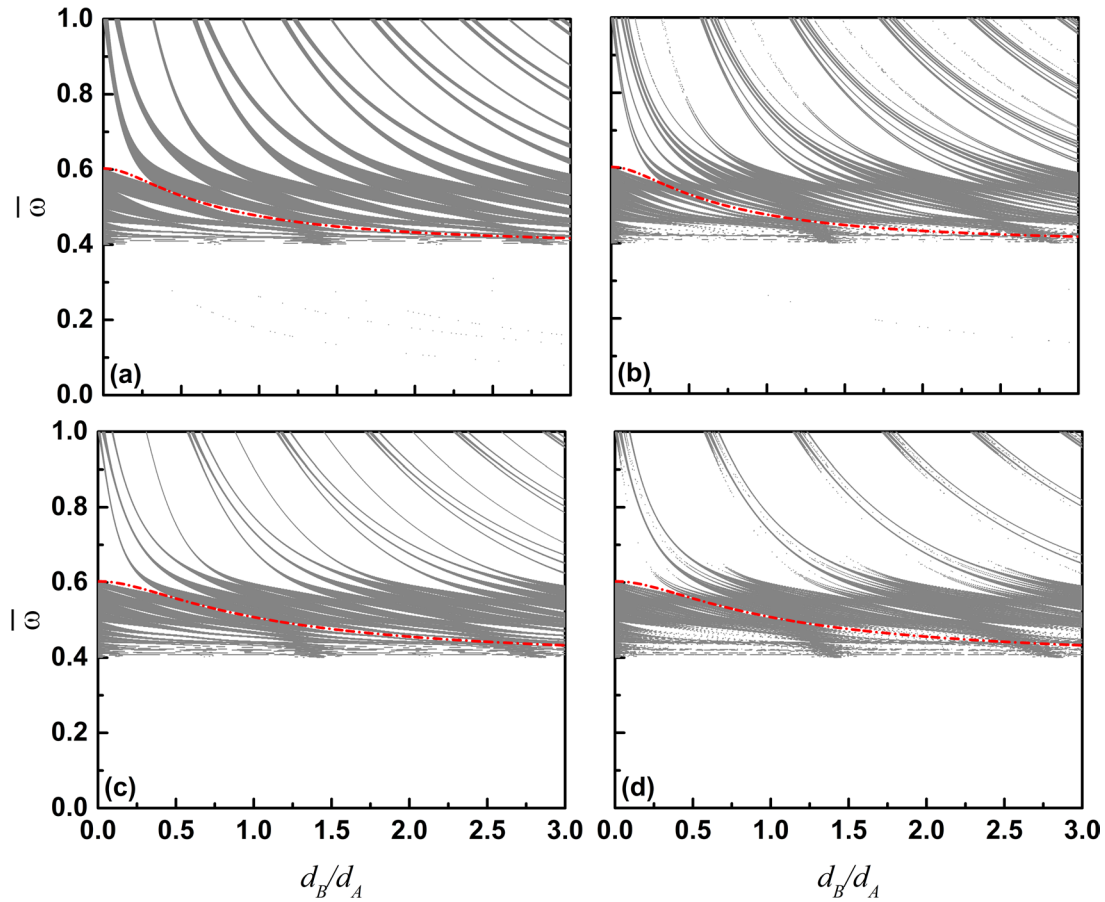


Figure 14. Same as figure 10, but for (a) second and (b) third generations of GTM(2,1), (c) second and (d) third generations of GTM(3,1) sequences.

critical value of reduced wave-vector \bar{k} , one can see that some backward waves turn into forward waves due to the influence of the dielectric over the metamaterial, same as it was found in figure 6.

In figures 7(b) and (c), we have the same as in figure 7(a), but for the second and third generation of the GTM(1,1) sequence, and their unit cells are, respectively, $3\text{GTM}(1,1) = |A|B|B|A|B|A|A|B|$ and $4\text{GTM}(1,1) = |A|B|B|A|B|A|A|B|B|A|A|B|A|B|B|A|$. One obtain similar conclusions as in figure 7(a), but now with a even more fragmented spectra. The reduced frequency for which the $\bar{n} = 0$ gap emerges for the GTM(1,1) sequence is $\bar{\omega} \approx 0.43$ (or 27.02 GHz). This value, in contrast with the GFSs, is the same for any generation of this sequence because the ratio between the number of slabs A and B is $N_A/N_B = p/q$ is constant for all generations. This is a very important property of the GTM sequences. Additionally, the frequency range for the omnidirectional band gap is $\bar{\omega} < 0.17$ for second and $\bar{\omega} < 0.18$ for third (or $\omega < 10.68$ and $\omega < 11.31$ GHz, respectively).

In figure 8, we present the photonic band structures for: (a) second ($2\text{GTM}(2,1) = |A|A|B|A|A|B|B|A|A|$) and (b) third ($3\text{GTM}(2,1) = |A|A|B|A|A|B|B|A|A|A|A|B|A|A|B|B|A|A|B|A|A|B|B|A|A|A|A| \dots \dots |A|B|A|A|B|$) generations of GTM(2,1), (c) second ($2\text{GTM}(3,1) = |A|A|A|B|A|A|A|B|A|A|A|B|B|A|A|A|$) and (d) third ($3\text{GTM}(3,1)$) generations of GTM(3,1). The unit

cell of the $3\text{GTM}(3,1)$ multilayer forms a too long chain of 64 letters A and B , and, because of that, we do not specify it here. However, the reader can obtain it from equations (25) and (26) or even from figure 3. Here, one can see the concentration of the bulk bands between $0.4 \leq \bar{\omega} \leq \bar{k}/\sqrt{\epsilon_A \mu_A}$ which is the only region where light can propagate in a infinite metamaterial. Some fewer bands outside this region are mainly inside the vacuum cone and this is due to the influence of the dielectric, despite the fact that they are almost imperceptible in even low generations. The second and third generations of the GTM(2,1), labels (a) and (b), likewise all previous structures, display a omnidirectional band gap for frequency regions of $\bar{\omega} < 0.18$ (or $\omega < 11.31$ GHz) and $\bar{\omega} < 0.26$ (or $\omega < 16.34$ GHz), but the second and third generations of the GTM(3,1), labels (c) and (d), present a complete band gap for $\bar{\omega} < 0.4$ (or $\omega < 25.13$ GHz), which consists in a omnidirectional band gap for both polarizations, in other words, a band gap independent of both incident angle and polarization of light, so that these structures behave as perfect Bragg's mirrors with very interesting applications such as solar energy [46] and dynamic pressure sensing [47]. Additionally, the frequency of the $\bar{n} = 0$ gap for the GTM(2,1) is $\bar{\omega} \approx 0.48$ and for the GTM(3,1) is $\bar{\omega} \approx 0.51$ (or $\omega \approx 30.16$ and 32.04 GHz, respectively).

From figure 9, where we present the photonic band structures for the same generations as in figure 8, but

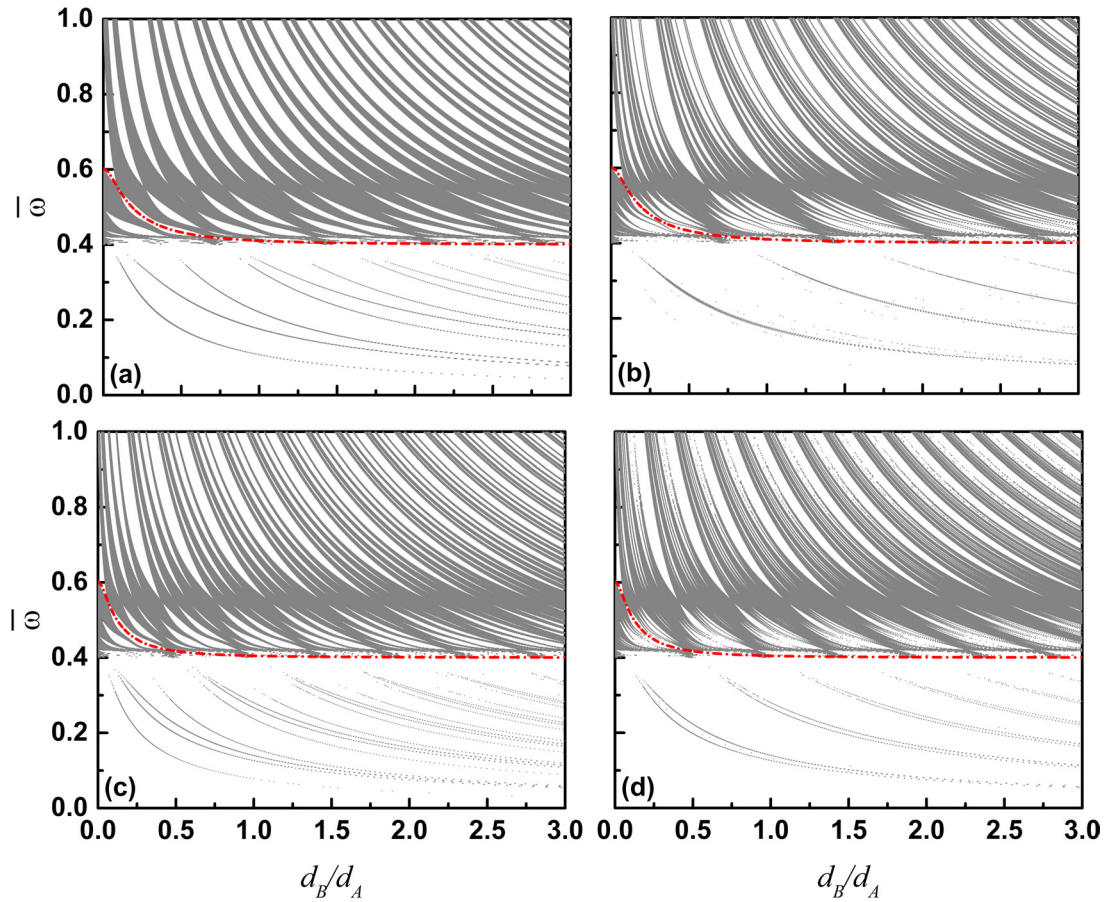


Figure 15. Same as figure 10, but for (a) second and (b) third generations of GTM(1,2), (c) second and (d) third generations of GTM(1,3) sequences.

now for GTM(1,2), in labels (a) and (b), and GTM(1,3), in labels (c) and (d). The unit cells of these structures are $2\text{GTM}(1,2) = |A|B|B|B|B|A|B|B|A|$, $3\text{GTM}(1,2) = |A|B|B|B|B|A|B|B|A|B|B|A|B|B|A|B|B|A|A|B|B|B|B|A|\cdots\cdots|B|B|A|A|B|B|$ and $2\text{GTM}(1,3) = |A|B|B|B|B|B|B|B|A|B|B|B|B|A|B|B|B|A|$. We do not present the unit cell for the $3\text{GTM}(1,3)$ for the same reason we explained about figure 8(d). Here, we observe several new branches that are narrower in comparison with others presented until now, but this fragmentation process occurs mainly in $\bar{\omega} < 0.4$ and $\bar{\omega} > 0.6$ frequency regions. This is a consequence of a greater influence of the dielectric medium, which has a predominant presence in the structure, as one can see in labels (d) and (e) from figure 3. The frequency for the $\bar{n} = 0$ gap is $\bar{\omega} \approx 0.41$ (or $\omega \approx 25.76$ GHz) for both GTM(1,2) and GTM(1,3) and this frequency almost corresponds to the resonance reduced frequency $\omega_0/\omega_p = 0.4$, that is also the lower limit of the NRI region. The omnidirectional band gaps emerge only for TE modes in the following frequency regions: $\bar{\omega} < 0.11$ (or $\omega < 6.91$ GHz) and $\bar{\omega} < 0.16$ (or $\omega < 10.05$ GHz) for second and third generations of GTM(1,2) and $\bar{\omega} < 0.08$ (or $\omega < 5.03$ GHz) and $\bar{\omega} < 0.13$ (or $\omega < 8.17$ GHz) for second and third generations of GTM(1,3).

In table 1 it is shown the frequencies of occurrence of the $\bar{n} = 0$ gap for each sequence while in table 2 it is presented the frequency range where there is an omnidirectional bandgap in TE modes in a summarized way. The complete

photonic bandgaps, that emerge for 2TM(3,1) and 3TM(3,1) multilayers are detached by using the symbol ^(a) in table 2.

In figures 10–15 we show the reduced frequency as a function of the ratio of the thicknesses of the materials d_B/d_A for the same generations of the generalized Fibonacci and Thue–Morse sequences displayed previously, considering the reduced wavelength equals to zero (normally incident wave) and a fixed value of d_A . In all these figures, the red dotted-dashed curve is the plot of equation (16) for each one of the quasiperiodic structures, i.e. the values of the reduced frequency $\bar{\omega}$ in which the $\bar{n} = 0$ gap requirement is satisfied as a function of the ratio d_B/d_A . The bands above this curve do not encounter the ones below for the following reason: when considering a superlattice whose constituents are PRI and NRI materials, there is always a frequency value that turn into zero the average refractive index, therefore forbidding light from crossing the structure, differently from gap closing, which are the points where the gap width vanishes [48].

In general, one have a similar behavior for all investigated sequences, that is, as the thickness of the dielectric increases, bulk bands above $\bar{\omega} > 0.6$ that once were in higher frequencies start to get narrower and move to a lower frequency region. As an example, the second generation of the GM, SM and BM sequences, presented in figures 4(a) and (b) (here we remind the reader that the 2SM structure is physically identical to the 3GM one) and 5(c) can be thought as a periodic structure

but with $d_B/d_A = 1, 2, 3$, respectively. So these bands shown in figures 4(b) and 5(c) are nothing but the bands shown in figure 4(a) that have flattened and shifted to lower frequencies. Also, as the generation number increases, the bands start to get fragmented but with the same general shape, due to the inherent characteristics of the long-range correlations of each quasiperiodic sequence. One can still observe that, for a same pair of the parameters (p, q) , the values of the reduced frequency $\bar{\omega}$, for which the $\bar{n} = 0$ gap occurs, asymptotically tends 0.41 as the ratio d_B/d_A increases, for both GFS and GTMS sequences. However, for $p < q$ (figures 12 and 15), the $\bar{\omega}$ goes to 0.41 faster than for $p = q$ (figures 10 and 13), and moreover, this case tends faster than for $p > q$ (figures 11 and 14). Besides, the frequencies for the $\bar{n} = 0$ gap, considering different generations, are almost or even exactly the same for Fibonacci SM and BM, GTM(1,1), GTM(1,2), GTM(1,3), GTM(2,1) and GTM(3,1) sequences, while they are quite different for Fibonacci GM, CM and NM sequences.

4. Conclusions

In this work we have studied the band structures of quasiperiodic multilayered photonic systems constructed according generalizations of two well know mathematical sequences: Fibonacci and Thue–Morse. The PCs are composed of slabs from two different media: one is a dispersive optical metamaterial, while the second is a non-dispersive dielectric (silicon dioxide, to be more specific). We have utilized the TMM for the theoretical approach and numerical simulations, which significantly simplifies the math of the problem. The band structure of a system is the most important source of physical information about that system, because it shows all values of frequency and the parallel component of the wave-vector that allows (bulk bands) or not (band gaps) transmission of the light wave through the structure. One can also know the direction of the energy flow by just looking at the slope of the plot, that is, if slope is positive (negative) the energy flow is in the same (opposite) direction of the propagation of light, where the backward waves are characteristics of metamaterials.

We have shown the frequency ranges for which the TE omnidirectional band gaps emerge for all structures presented, except for the GTM(3,1) structures that, instead, present a complete band gap, which is a omnidirectional band gap independent of polarization, with various practical and technological applications. We also studied and presented the frequencies in which the $\bar{n} = 0$ band gap occurs, that is only possible when metamaterials are considered. For the GFS sequences the position of this gap changes for each generation while for GTMS ones it does not. Another very interesting result is the higher concentration of the pass bands inside (outside) the $n_A < 0$ region when there are more (less) blocks A, metamaterial, than B, dielectric, in the unit cell. Additionally, we have presented an analytical expression for the frequency of occurrence of the $\bar{n} = 0$ gap as a function of the thicknesses ratio d_B/d_A and the plot of $\bar{\omega}$ versus d_B/d_A for normally incident waves. So, we concluded that the values of the reduced frequency $\bar{\omega}$, for which the $\bar{n} = 0$ gap occurs, asymptotically

tends 0.41 as the ratio d_B/d_A increases, independent of the sequences.

Some of the very exciting and amazing applications of photonic structures based on PRI and NRI materials which have been recently investigated are superlens, NRI and invisibility cloak [49, 50]; digital metamaterials [51]; among others [52]. Therefore, all multilayered structures considered in this work can be realized and investigated experimentally and we hope that our results can motivate experimental research groups to study them.

Acknowledgments

BPS and CHC would like to thank the Brazilian Research Agencies CNPq (Grant No. 429299/2016-8). CHC also thanks to FUNCAP (Grant No. BP3-0139-00177.01.00/18) for their financial support. Also, we would like to thank the Prof Dr Lindberg L Gonçalves (from Federal University of Ceará) for reviewing and giving valuable comments which helped to improve the manuscript.

ORCID iDs

Bruno P Silva  <https://orcid.org/0000-0001-7113-4928>
 Carlos H Costa  <https://orcid.org/0000-0002-4835-9392>

References

- [1] Steurer W and Widmer D S 2007 *J. Phys. D: Appl. Phys.* **40** R229
- [2] Sakoda K 2005 *Optical Properties of Photonic Crystals* 2nd edn (Berlin: Springer)
- [3] Joannopoulos J D, Johnson S G, Winn J N and Meade R D 2011 *Photonic Crystals: Molding the Flow of Light* 2nd edn (Princeton, NJ: Princeton University Press)
- [4] Soukoulis C M (ed) 1996 *Photonic Band Gap Materials* (Dordrecht: Kluwer)
- [5] Veselago V G 1968 *Sov. Phys.—Usp.* **10** 509
- [6] Ramakrishna S A 2005 *Rep. Prog. Phys.* **68** 449
- [7] Foteinopoulou S, Economou E N and Soukoulis C M 2003 *Phys. Rev. Lett.* **90** 107402
- [8] Shelby R A, Smith D R and Schultz S 2001 *Science* **292** 77
- [9] Smith D R, Schultz S, Marko P and Soukoulis C M 2002 *Phys. Rev. B* **65** 195104
- [10] Soukoulis C M, Kafesaki M and Economou E N 2006 *Adv. Mater.* **18** 1941
- [11] Gong Q and Hu X (ed) 2014 *Photonic Crystals: Principles and Applications* (Stanford, CA: Pan Stanford)
- [12] dal Negro L (ed) 2013 *Optics of Aperiodic Structures: Fundamentals and Device Applications* (Boca Raton, FL: Pan Stanford Publishing)
- [13] Maciá E 2006 *Rep. Prog. Phys.* **69** 397
- [14] Lee C-C (ed) 2015 *The Current Trends of Optics and Photonics* (Berlin: Springer)
- [15] Shechtman D, Blech I, Gratias D and Cahn J W 1984 *Phys. Rev. Lett.* **53** 1951
- [16] Steurer W and Deloudi S 2009 *Crystallography of Quasicrystals—Concepts, Methods and Structures (Springer Series in Materials Science vol 126)* (Berlin: Springer)

- [17] Araújo C A A, Albuquerque E L, Mauriz P W and Vasconcelos M S 2009 *J. Opt. Soc. Am. B* **26** 1129
- [18] de Medeiros F F, Albuquerque E L, Vasconcelos M S and Farias G A 2006 *Surf. Sci.* **600** 4337
- [19] Araújo C A A, Albuquerque E L, Anselmo D H A L and Vasconcelos M S 2008 *Phys. Lett. A* **372** 1135
- [20] Vasconcelos M S and Albuquerque E L 1998 *Phys. Rev. B* **57** 2826
- [21] Albuquerque E L and Cottam M G 2004 *Polaritons in Periodic and Quasiperiodic Structures* (Amsterdam: Elsevier)
- [22] Costa C H O and Vasconcelos M S 2013 *J. Phys.: Condens. Matter* **25** 286002
- [23] Maciá E 2012 *Rep. Prog. Phys.* **75** 036502
- [24] Kolá M, Ali M K and Nori F 1991 *Phys. Rev. B* **43** 1034
- [25] de Spinadel V W 1999 *Nonlinear Anal.* **36** 721
- [26] Sánchez-Soto L L, Monzón J J, Barriuso A G and Cariñena J F 2012 *Phys. Rep.* **513** 191.
- [27] Lee H-Y and Yao T 2003 *J. Appl. Phys.* **93** 819
- [28] Pérez-Huerta J S, Ariza-Flores D, Castro-García R, Mochán W L, Ortiz G P and Agarwal V 2018 *Int. J. Mod. Phys. B* **32** 1850136
- [29] Pendry J B and Smith D R 2004 *Phys. Today* **57** 37
- [30] Markoš P and Soukoulis C M 2008 *Wave Propagation: from Electrons to Photonic Crystals and Left-Handed Materials* (Princeton, NJ: Princeton University Press)
- [31] Vasconcelos M S, Mauriz P W, de Medeiros F F and Albuquerque E L 2007 *Phys. Rev. B* **76** 165117
- [32] Brandão E R, Vasconcelos M S, Albuquerque E L and Fulco U L 2017 *Opt. Mater.* **64** 126
- [33] Yeh P 2005 *Optical Waves in Layered Media* 2nd edn (New York: Wiley)
- [34] Albuquerque E L and Cottam M G 1993 *Phys. Rep.* **233** 67
- [35] Barber E M 2008 *Aperiodic Structures in Condensed Matter: Fundamentals and Applications* (Boca Raton, FL: CRC Press)
- [36] Kocaman S, Chatterjee R, Panoiu N C, McMillan J F, Yu M B, Osgood R M, Kwong D L and Wong C W 2009 *Phys. Rev. Lett.* **102** 203905
- [37] Kocaman S, Aras M S, Hsieh P, McMillan J F, Biris C G, Panoiu N C, Yu M B, Kwong D L, Stein A and Wong C W 2011 *Nat. Photon.* **5** 499
- [38] Maciá E 2017 *Ann. Phys., NY* **529** 1700079
- [39] Vasconcelos M S, Albuquerque E L and Mariz A M 1998 *J. Phys.: Condens. Matter* **10** 5839
- [40] Notomi M 2010 *Rep. Prog. Phys.* **73** 096501
- [41] Singh P, Tripathi D Kr, Jaiswal S and Dixit H K 2014 *Adv. Opt. Technol.* **2014** 275083
- [42] Salmanpour A, Mohammadnejad S and Bahrami A 2015 *Opt. Quant. Electron.* **47** 2249
- [43] Hussein H M E, Ali T A and Rafat N H 2018 *Opt. Commun.* **411** 175
- [44] Daghooghi T, Soroosh M and A-Asl K 2018 *Photon. Netw. Commun.* **35** 335
- [45] Nusinsky I and Hardy A A 2007 *Appl. Opt.* **46** 3510
- [46] Estrada-Wiese D, del Ríon J A, Nava R, Gómez-Ocampo J, Tagüeña-Martínez J and Montiel-González Z 2015 *Sol. Energy Mat. Sol. C* **141** 315
- [47] Lee G, Scripka D A, Wagner B, Thadhani N N, Kang Z and Summers C J 2017 *Opt. Express* **25** 27067
- [48] Nusinsky I and Hardy A A 2006 *Phys. Rev. B* **73** 125104
Nusinsky I and Hardy A A 2008 *Phys. Rev. B* **77** 199901
- [49] Monticone F and Alù A 2017 *Rep. Prog. Phys.* **80** 036401
- [50] Wong Z J, Wang Y, O'Brien K, Rho J, Yin X, Zhang S, Fang N, Yen T-J and Zhang X 2017 *J. Opt.* **19** 084007
- [51] Giovampaola C D and Engheta N 2014 *Nat. Mater.* **13** 1115
- [52] Koenderink A F, Alù A and Polman A 2015 *Science* **348** 516